Copy No.

NASA Project Apollo Working Paper No. 1091

A METHOD FOR DETERMINING AERODYNAMIC DAMPING OF THE STRUCTURAL BENDING MODES WITH APPLICATION TO THE APOLLO/SATURN I LAUNCH VEHICLE

NATIONAL AERONAUTICS AND SPACE ADMINISTRATION
MANNED SPACECRAFT CENTER
Houston, Texas

September 27, 1963

NASA PROJECT APOLLO WORKING PAPER NO. 1091

A METHOD FOR DETERMINING AERODYNAMIC DAMPING OF THE STRUCTURAL BENDING MODES WITH APPLICATION TO THE APOLLO/SATURN I LAUNCH VEHICLE

Prepared by: May T. Meadows
May T. Meadows
AST, Fluid and Flight Mechanics

Authorized for Distribution:

Warren Gillespie, Jr.
for Maxime A. Faget
Assistant Director
for Engineering and Development

NATIONAL AERONAUTICS AND SPACE ADMINISTRATION

MANNED SPACECRAFT CENTER

HOUSTON, TEXAS

September 27, 1963

TABLE OF CONTENTS

LIST OF FIGURES

A METHOD FOR DETERMINING AERODYNAMIC DAMPING OF THE STRUCTURAL BENDING MODES WITH APPLICATION TO THE APOLLO/SATURN I LAUNCH VEHICLE

SUMMARY

Calculation of the aerodynamic damping of the Apollo/Saturn I Launch Vehicle has been made for the first two structural bending modes. A comparison of the damping derivative with wind tunnel data indicates that this method is valid for analytic determination of the aerodynamic damping for a vehicle of this type.

INTRODUCTION

Air forces due to the n^{th} modal velocity are generally negligible compared to structural design airloads but provide a beneficial source of damping on the n^{th} mode itself. In the case of a finned body such as the Apollo/Saturn I the aerodynamic damping can be larger than the structural damping and of considerable importance.

The modal velocity induces small changes in angle of attack along the vehicle. The distribution of lift due to the changes in angle of attack may be determined by slender body theory (with some modification for the command module). From this lift distribution, the generalized force is determined for the modal differential equation. The ratio of aerodynamic damping to critical damping as a function of Mach number is found from this equation.

This paper presents a technique for obtaining the aerodynamic damping from the modal velocity. Application of this technique to the Apollo/Saturn I configuration consists of calculations made for a specific time in the flight trajectory and extension of these calculations to other times of interest.

SYMBOLS

C_{N_α}	Normal force coefficient per unit angle of attack, 1/deg
F_{y_n}	Generalized force associated with mode n, lb
L	Vehicle length, in.
M	Mass. $\frac{\text{lb-sec}^2}{\text{ft}}$
M_n	Generalized mass
N	Normal force, lb
n	Mode number
q	Free-stream dynamic pressure lb/ft^2
S(x)	Reference area of vehicle as a function of x, in.^2
t	Time, sec
V	Velocity, ft/sec
x	Distance along vehicle (zero at the nozzle end), in.
$y_n(x,t)$	Deflection in mode n
α	Angle of attack, radians
β	Damping coefficient
ρ	Stream density, slug/ft^3
ω	Modal frequency, rad/sec

Subscripts

A	Aerodynamic
cr	Critical

S Structural

n Modal number

ANALYSIS

Method

Sketch (a) presents the Apollo/Saturn I vehicle as deflected in the first free-free bending mode. Displacements and velocities in each structural mode induce aerodynamic forces on the vehicle due to local angle of attack along the vehicle. For modal displacement $\alpha = \frac{-dy_n(x)}{dx}$.

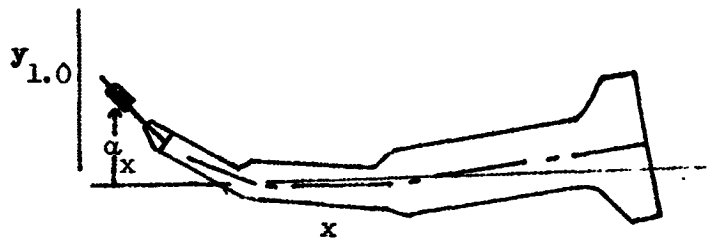

Sketch (a)

The aerodynamic force distribution due to $\frac{dy_n(x)}{dx}$ for slender missiles is small and does not affect damping; therefore, it is neglected for this vehicle.

The change in local angle of attack α_x due to modal velocity produces normal force loads that induce aerodynamic damping. Although these loads are small for vehicles such as the Apollo/Saturn I, they can produce a significant amount of damping. This damping is dependent on the vehicle configuration, modal shape and modal frequency. A drawing of the Apollo/Saturn I launch vehicle is given in figure 1.

The local angle of attack α_x due to modal velocity can be approximated, provided α is small, by:

$$\alpha_{x_n} = \frac{-\dot{y}_n(x)}{V} \qquad (1)$$

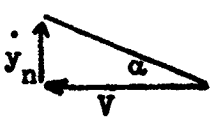

The modal displacement y_n when normalized can be written as:

$$y_n(x,t) = y_n(x)\sin \omega_n t \qquad (2)$$

so that

$$\dot{y}_n(x,t) = \omega_n y_n(x) \cos \omega_n t$$

For $t = 0$ or maximum value of $\dot{y}_n$

$$\dot{y}_n(x) = \omega_n y_n(x) \tag{3}$$

Thus, substituting (3) in (1)

$$\alpha_{x_n} = \frac{-\omega_n y_n(x)}{V} \tag{4}$$

The distribution of lift for small changes in α caused by $\dot{y}_n(x)$ may be determined by use of slender body theory for bodies of revolution (ref. 1)

$$N = 2\alpha_n qS \tag{5}$$

so that

$$\frac{dN}{dx} = 2q \frac{d}{dx}(\alpha_n S)$$

or

$$\frac{dN}{dx} = \frac{-2q\omega_n}{V} \frac{d}{dx}(y_n S) \tag{6}$$

or

$$\frac{dN}{dx} = -\rho V \omega_n \frac{d}{dx}(y_n S) \tag{6a}$$

This equation shows that the lift due to modal velocity is a function of the forward velocity of the vehicle instead of the square of the velocity, as expected.

Lift Calculations

In order to calculate this normal force along the vehicle, parameters from the SA-5 trajectory, as given in reference 2, were used with modal shapes and frequencies calculated in a digital program for a particular time. The time selected was for maximum dynamic pressure, 67 seconds after lift off. The dynamic pressure was multiplied by 1.2 in order to take into account possible deviations from the nominal trajectory. The

first two bending modes normalized at the nose are shown plotted in figures 2 and 3. The important data associated with this case for t = 67 seconds are:

$$\text{Mach No.} = 1.55$$

$$q = 864 \text{ lb/ft}^2$$

$$V = 1{,}400 \text{ ft/sec}$$

$$\omega_1 = 11.32 \text{ rad/sec}$$

$$\omega_2 = 23.03 \text{ rad/sec}$$

The lift distribution is shown plotted in figures 4 and 5. The data points shown on these figures are from wind tunnel tests on the Command Module and were used for the lift distribution. The generalized force due to modal velocity is

$$F_{\dot{y}_n} = \int_0^L \frac{dN}{dx} y_n(x) dx \tag{7}$$

In order to determine the damping due to unit modal velocity, the generalized force must be divided by the modal frequency ω_n giving

$$\frac{F_{\dot{y}_n}}{\omega_n} = \frac{1}{\omega_n} \int_0^L \frac{dN}{dx} y_n(x) dx \tag{8}$$

Calculations for the first two modes were made to determine $\frac{F_{\dot{y}_n}}{\omega_n}$ for the time t = 67 seconds.

The first two modes for t = 67 seconds given in figures 2 and 3 were assumed to be constant over the Mach range of interest, M = 0.7 to M = 1.55. Using this assumption $\frac{F_{\dot{y}_n}}{\omega_n}$ was calculated for these Mach numbers by using the ratio of $\frac{q}{V}$ along the flight trajectory to the $\frac{q}{V}$ value at M = 1.55. The generalized forces due to unit modal frequency, excluding fins are:

$$\frac{F_{\dot{y}_1}}{\omega_1} = -1.2413$$

and

$$\frac{F_{y_2}}{\omega_2} = -1.0869$$

The lift for the fins due to local angle of attack change was obtained separately using the C_{f_α} for M = 1.55 obtained from wind tunnel tests (ref. 5). This value was determined by taking the difference in C_{n_α} on the vehicle with fins and C_{n_α} on the vehicle without fins at M = 1.55. For M = 1.55

$$C_{n_\alpha} = 0.057 \ \frac{1}{\text{deg}} \quad \text{(Based on } S = 360 \text{ ft}^2\text{)}$$

Center of pressure of fin = 173 inches from station 0

$$\alpha_n = \frac{-\omega_n \, y_n(173)}{V}$$

$$\alpha_1 = \frac{-11.32(.095)}{16,800} = -0.00006064 \text{ (1st mode)}$$

$$\alpha_2 = \frac{-23.03(-.14)}{16,800} = 0.000192 \text{ (2nd mode)}$$

Dividing through by ω_n, the concentrated lift forces on the fin become:

$$\frac{N_1}{\omega_1} = \frac{(.056)(57.3)(-0.00006064)(864)(360)}{11.32}$$

$$= -5.37 \ \frac{\text{lb}}{\text{rad/sec}}$$

and

$$\frac{N_2}{\omega_2} = \frac{(.056)(57.3)(0.000192)(864)(360)}{23.03}$$

$$= 8.28 \ \frac{\text{lb}}{\text{rad/sec}}$$

Lift due to the fins is given as concentrated force at the fin center of pressure in figures 4 and 5. Generalized forces due to unit modal frequency on the fin:

$$\frac{F_{\dot{y}_n}}{\omega_n} = \left[\frac{N_n}{\omega_n}\right]\left[y_n(173)\right]$$

Thus

$$\frac{F_{\dot{y}_1}}{\omega_1} = -5.37\ (0.093)$$

$$= -0.505$$

and

$$\frac{F_{\dot{y}_2}}{\omega_2} = 8.28\ (-0.14)$$

$$= -1.1592$$

Total generalized forces due to unit modal frequency:

$$\frac{F_{\dot{y}_n}}{\omega_n} = \frac{I_{\dot{y}_n}}{\omega_{n(\text{along vehicle})}} + \frac{F_{\dot{y}_n}}{\omega_{n(\text{fins})}}$$

$$\frac{F_{\dot{y}_1}}{\omega_1} = -1.24[5] - 0.505$$

$$= -1.74[5]$$

and

$$\frac{F_{\dot{y}_2}}{\omega_2} = -1.0869 - 1.1592$$

$$= -2.244$$

A form of the generalized equation of motion for elastic modes is:

$$M_n \ddot{y}_n = -\omega_n^2 M_n y_n + \frac{F_{\dot{y}_n}}{\omega_n} \dot{y}_n$$

where M_n = generalized mass = $\int_0^L M(x) y_n^2(x)dx$

and $M(x)$ = distributed mass

Thus, the generalized equations become:

$$18.708\,\ddot{y}_1 + 1.746\,\dot{y}_1 + (11.32)^2\,(18.708)y_1 = 0 \qquad (M_1 = 18.708)$$

and

$$22.11\,\ddot{y}_2 + 2.244\,\dot{y}_2 + (25.04)^2\,(22.11)y_2 = 0 \qquad (M_2 = 22.11)$$

The ratio of aerodynamic damping to critical damping is shown in the following differential equation (ref. 4):

$$M_n \ddot{y}_n - \frac{F_{\dot{y}_n}}{\omega_n} \dot{y}_n + \omega_n^2 M_n y_n = 0 \qquad \text{Let } \beta = -\frac{F_{\dot{y}_n}}{\omega_n} = \text{coefficient of damping term}$$

In operator form

$$D^2 + \frac{\beta}{M_n} D + \omega_n^2 = 0$$

$$D = \frac{-\frac{\beta}{M_n} \pm \sqrt{\frac{\beta^2}{M_n^2} - 4\omega_n^2}}{2}$$

whose solution is:

$$y_n = K_1 e^{\left(-\frac{\beta}{2M_n} + \frac{1}{2}\sqrt{\frac{\beta^2}{M_n^2} - 4\omega_n^2}\right)t} + K_2 e^{\left(-\frac{\beta}{2M_n} - \frac{1}{2}\sqrt{\frac{\beta^2}{M_n^2} - 4\omega_n^2}\right)t}$$

or

$$y_n = Ce^{-\frac{\beta}{2M_n}t}\left(A \sin\sqrt{\omega_n^2 - \frac{\beta^2}{4M_n^2}}\,t + \beta \cos\sqrt{\omega_n^2 - \frac{\beta^2}{4M_n^2}}\,t\right)$$

The behavior of the damped system depends upon whether the radical of this equation has a value which is real, imaginary, or zero. For a critical damping coefficient β_{cr} the value of the radical must be zero,

or $\beta_{cr} = 2\omega_n M_n$

The amount of damping in the system is then determined by the ratio

$$\beta/\beta c = \frac{\beta}{2\omega_n M_n} = -\frac{F_{y_n}}{\omega_n}\Big/ 2\omega_n M_n$$

For the first mode, this becomes

$$\frac{\beta}{\beta_{cr}} = \frac{1.746}{2(11.32)(18.708)} = 0.0041$$

The second mode gives

$$\frac{\beta}{\beta_{cr}} = \frac{2.244}{2(23.03)(22.109)} = 0.0021$$

These values are plotted in figure 6 for $M = 1.55$, along with the values calculated for the Mach numbers considered.

The values for the other Mach numbers were obtained by multiplying the generalized force along the vehicle value for $M = 1.55$ by the ratio

$$\frac{q/V \text{ Mach No.} = 0.7, 0.8, \ldots 1.5}{q/V \text{ Mach No.} = 1.5}$$

The generalized force values for the fins were obtained in the same manner; however, the variation of C_{n_α} of the fins with Mach number was also taken into account.

RESULTS

The ratio of aerodynamic damping to critical damping is presented in figure 6. Also in this figure are the results from the Langley SD-1 shake test on the Apollo/Saturn I configuration (unpublished data). The following results may be noted:

1. The structural damping (as indicated by the dashed line) is only a small percentage of the total damping for both the calculated values and the tests results for the model investigated.

2. An increase in the calculated aerodynamic damping at Mach number 1.0 is due primarily to an increase of the C_{n_α} of the fins in this area. This increase in damping does not appear in the experimental results. The overall difference in magnitude of the calculated and experimental results may be attributed in part to the difference in trajectory parameters and modal shapes.

3. The result of a study on separated flow effects on the Saturn I is given in reference 5. This study indicated that the separated flow along the vehicle has a large effect on the steady and unsteady loads. Calculations using these loads give a larger percent of aerodynamic damping than those plotted in figure 6, particularly in the second mode. Part of this increased damping is due to the large positive load on the Command Module induced from the wake of the disk on the escape rocket. Since the disk has been removed from the tower configuration there would be a corresponding decrease in the aerodynamic damping as determined in reference 5. The remaining difference cannot be fully accounted for without a review of the calculations used to determine the damping in reference 5.

CONCLUDING REMARKS

The method used appears to be a valid approach for the determination of aerodynamic damping on the Saturn I. Damping in the first mode due to the aerodynamic effect is of a much larger magnitude than the structural damping, with the largest amount being at Mach number 1.0. The second mode damping calculations show a smaller ratio of aerodynamic damping to structural damping; however, this amount would still constitute appreciable damping in the second mode.

REFERENCES

1. Ferri, Antonio: Elements of Aerodynamics of Supersonic Flows. The Macmillan Company, 1949, pp. 216-220.

2. C-1 Design Criteria Manual.

3. Air Load Manual Saturn C-1 Block II. Sheet No. 5.111.

4. Freberg, C. R., Kemler, E. N.: Elements of Mechanical Vibration. John Wiley and Sons, Inc., 1957, pp. 41-55.

5. Ericsson, Lars-Eric, and Reding, J. P.: Separated Flow Effects on the Aeroelastic Stability of the Saturn-Apollo Accent Vehicle. Lockheed Missiles and Space Company, Sunnyvale, California, (Preliminary Report).

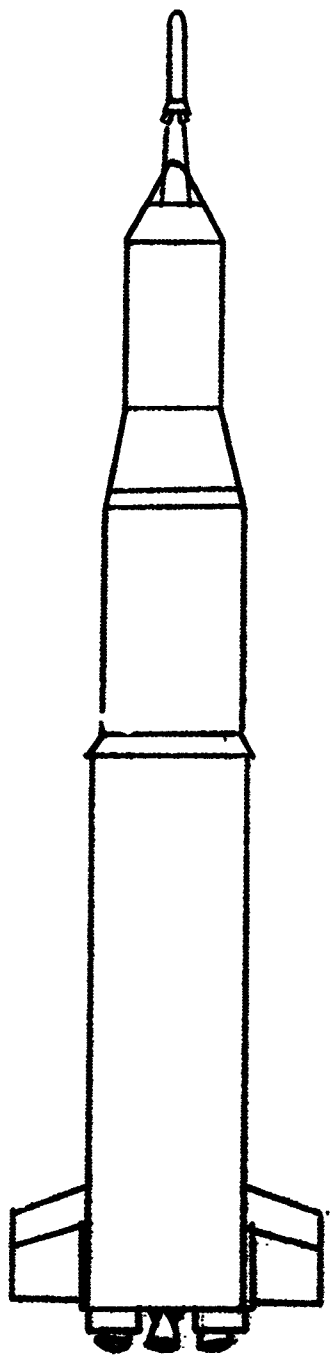

Figure 1.- Saturn-Apollo launch vehicle.

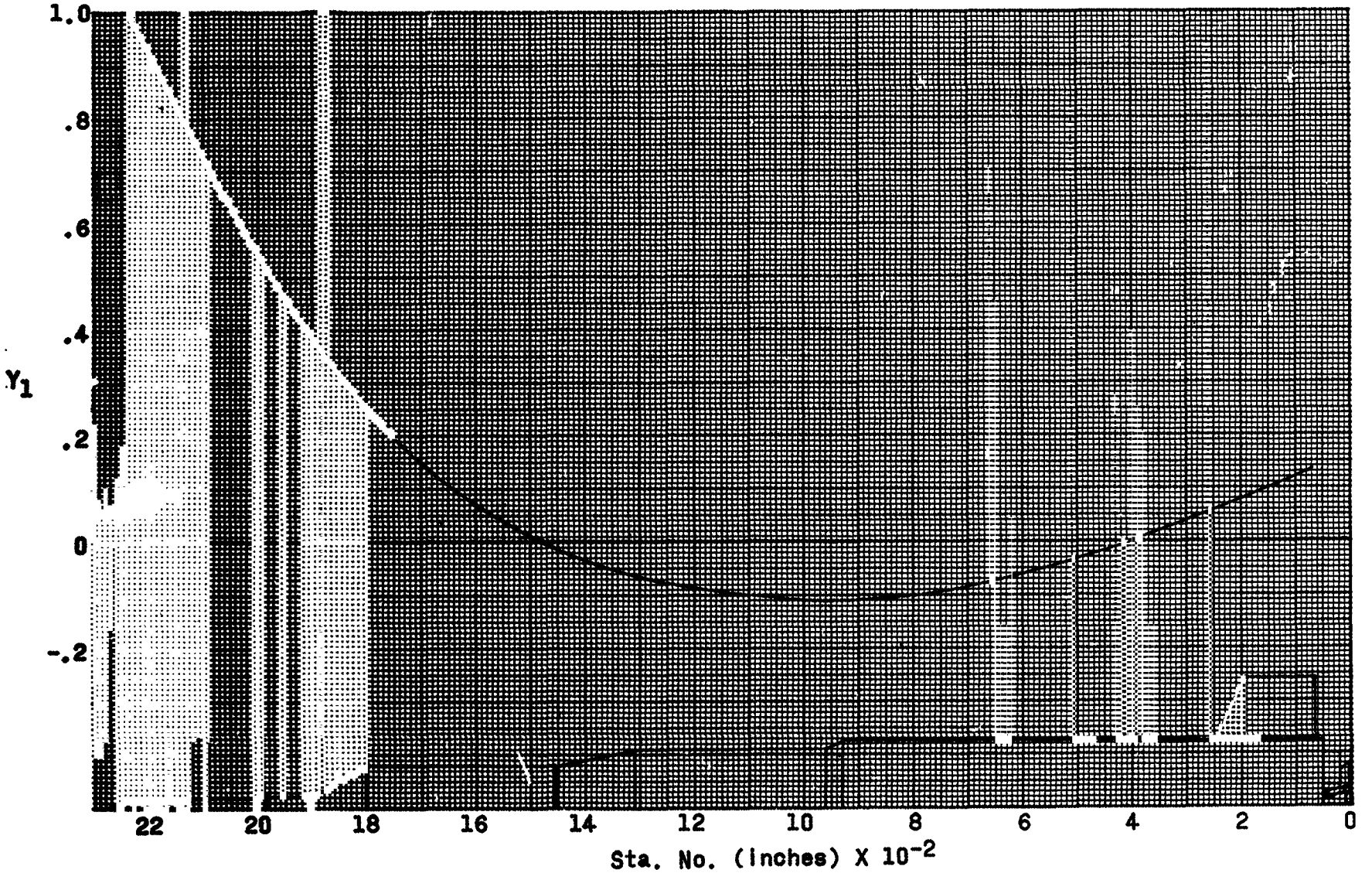

Figure 2.- First mode deflection (t = 67 sec). ω_1 = 11.32 rad/sec.

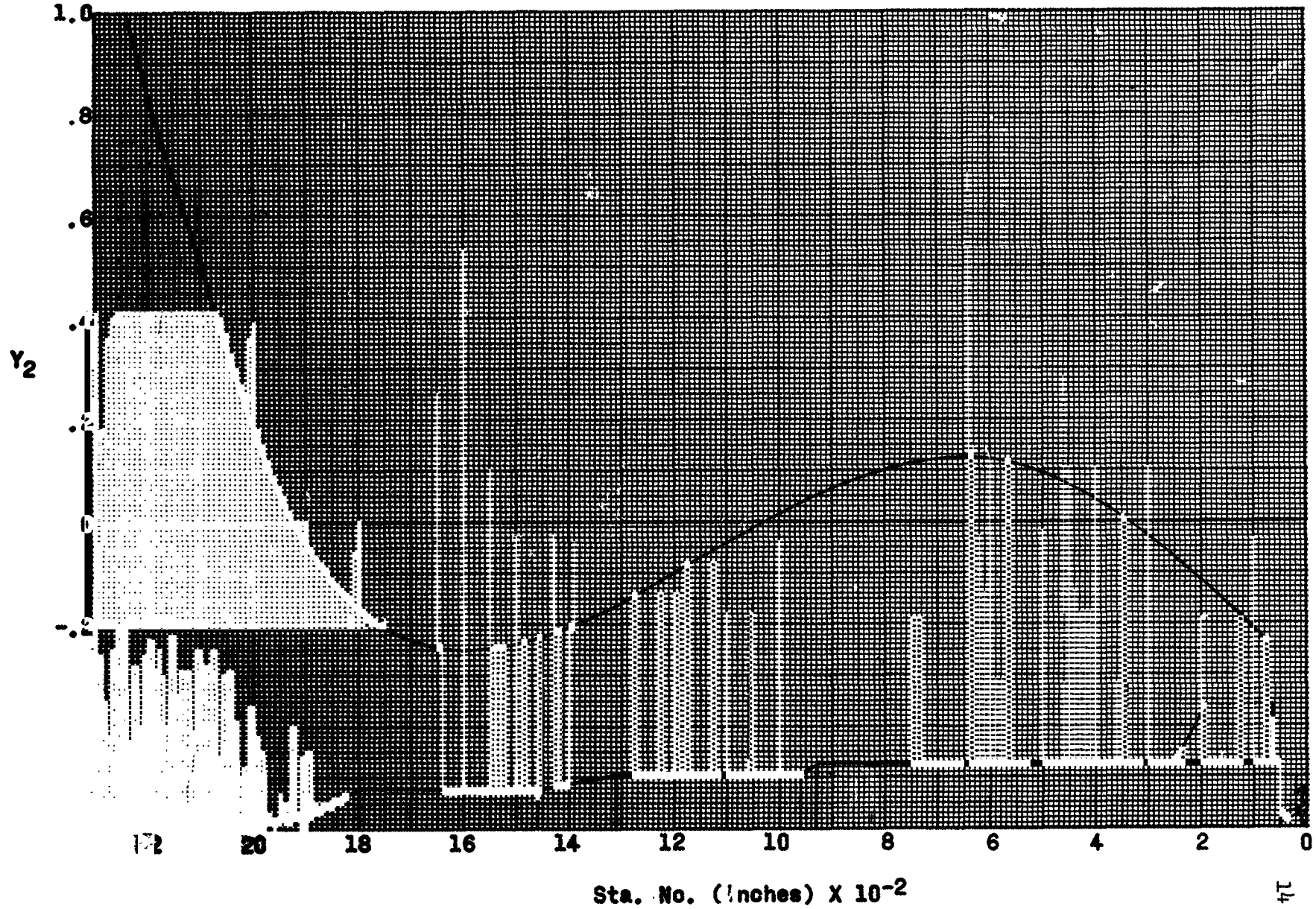

Figure 3.- Second mode deflection (t = 67 sec). ω_2 = 23.03 rad/sec.

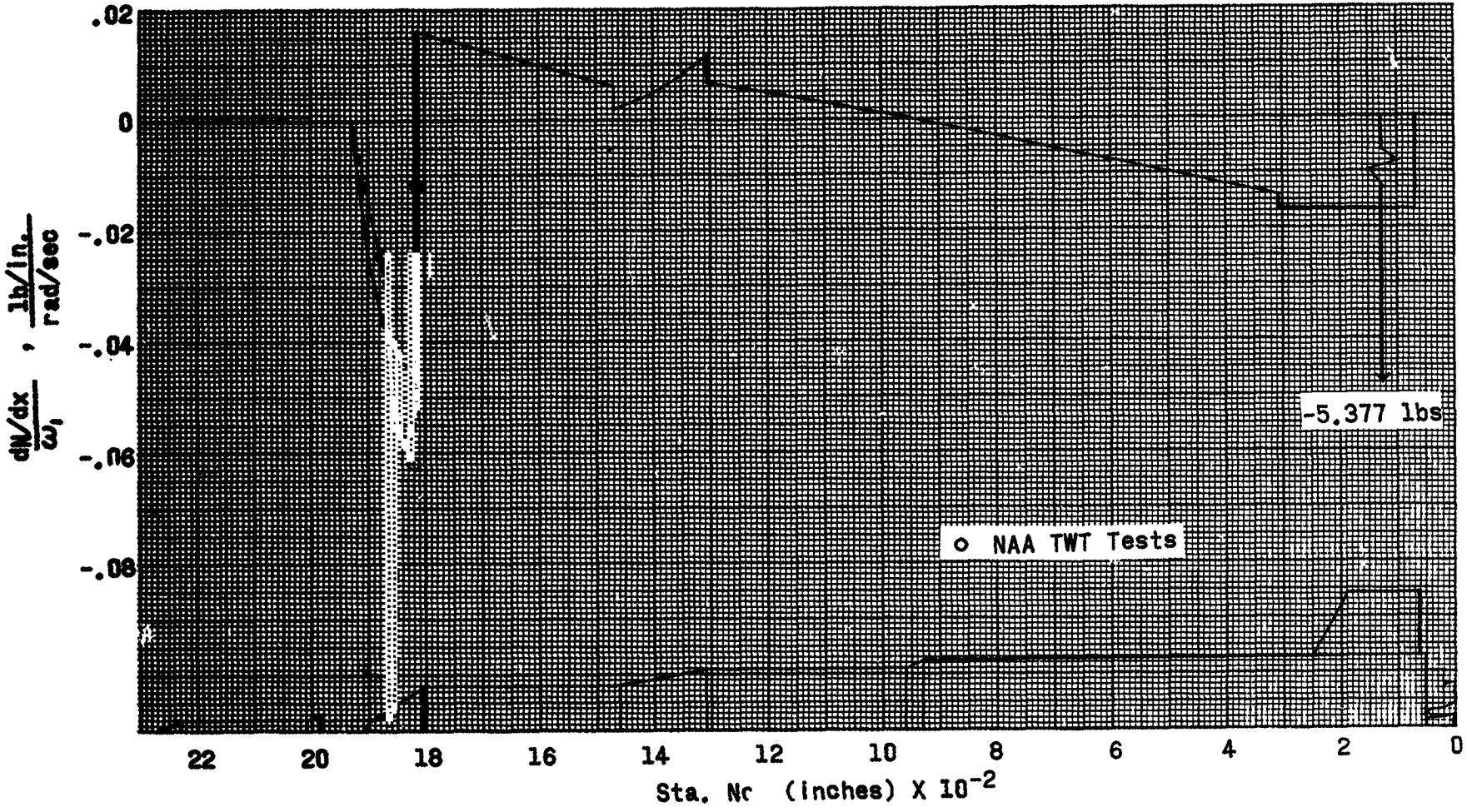

Figure 4.- Lift due to first mode velocity.

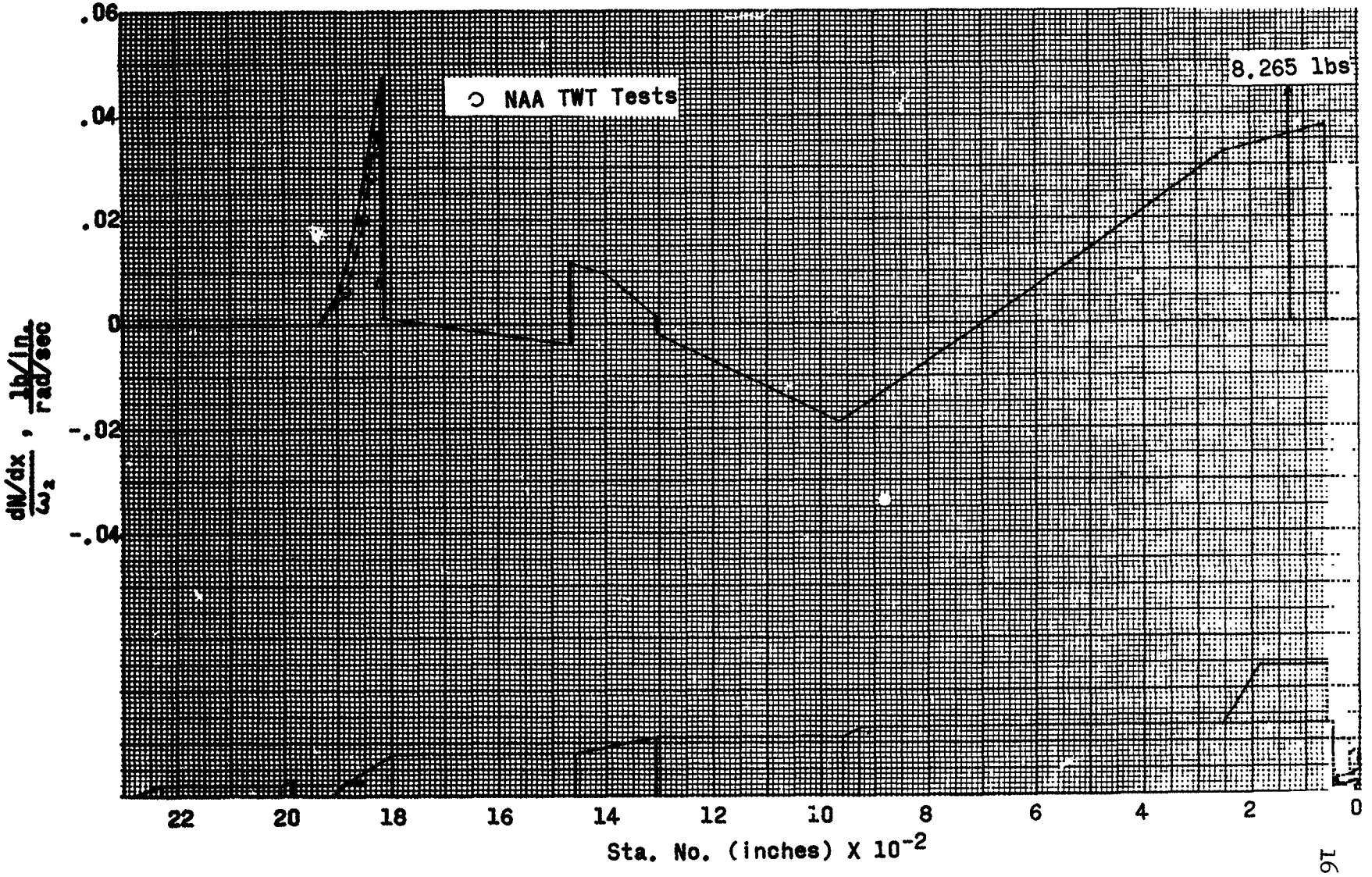

Figure 5.- Lift due to second mode velocity.

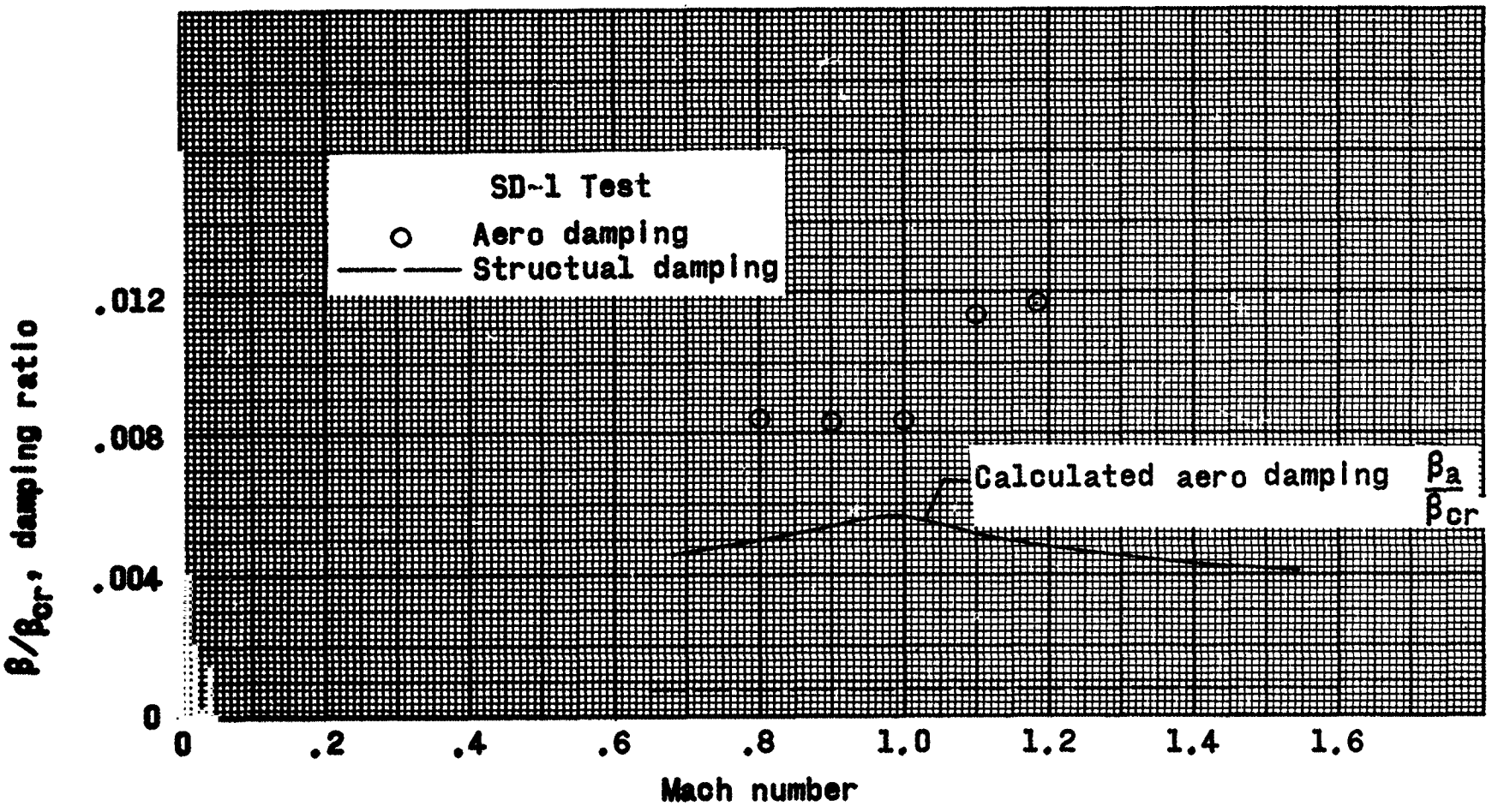

(a) First free-free mode

Figure 6.- Variation of damping with Mach number.

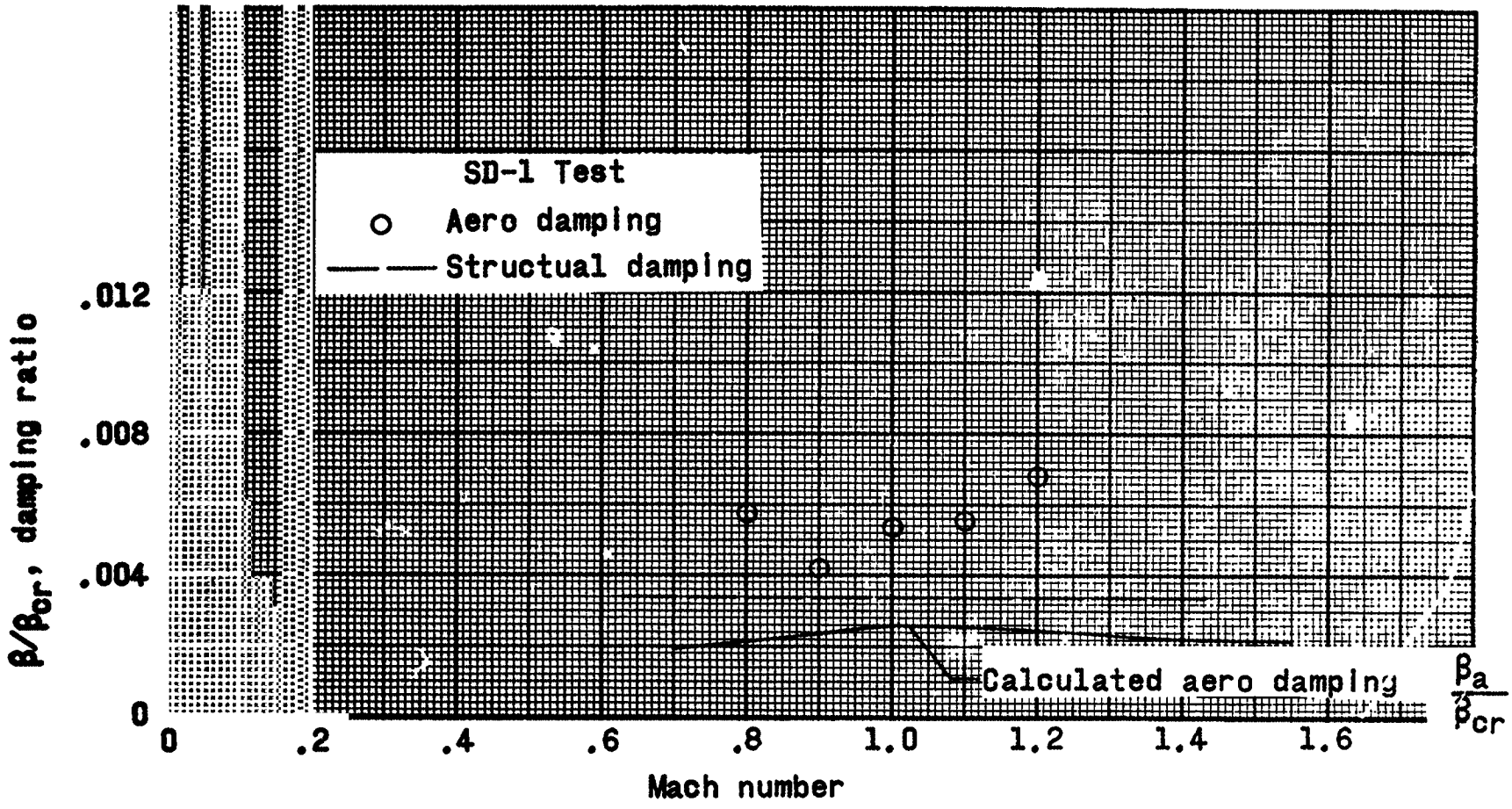

(b) Second free-free mode

Figure 6.- Concluded.